Journal of Inorganic Biochemistry 191 (2019) 164–173

Contents lists available at ScienceDirect

Journal of Inorganic Biochemistry

journal homepage: www.elsevier.com/locate/jinorgbio

Evaluation of PTA-derived ruthenium(II) and iridium(III) quinoline complexes against chloroquine-sensitive and resistant strains of the *Plasmodium falciparum* malaria parasite

Tameryn Stringer[a], Maria Alejandra Silva Quintero[a], Lubbe Wiesner[b], Gregory S. Smith[c,*], Ebbe Nordlander[a,*]

[a] Chemical Physics, Department of Chemistry, Lund University, Box 124, SE-221 00 Lund, Sweden
[b] Division of Clinical Pharmacology, Department of Medicine, University of Cape Town, Observatory 7925, Cape Town, South Africa
[c] Department of Chemistry, University of Cape Town, Rondebosch 7701, Cape Town, South Africa

ARTICLE INFO

Keywords:
Plasmodium falciparum
Ruthenium
Iridium
Quinoline
1,3,5-Triaza-phosphaadamantane
Antiplasmodial activity

ABSTRACT

Cationic 1,3,5-triaza-phosphaadamantane (PTA) quinoline ruthenium(II) and iridium(III) complexes were successfully synthesized and characterized using standard spectroscopic and analytical techniques. The complexes were evaluated for their *in vitro* antiplasmodial activities against the chloroquine-sensitive (CQS) NF54 and chloroquine-resistant (CQR) K1 strains of the *Plasmodium falciparum* species of the malaria parasite and were found to exhibit good activities in the sensitive strain but moderate activities in the resistant strain, suggesting a resistance mechanism similar to chloroquine (CQ). Selected samples were screened for their ability to inhibit synthetic haemozoin formation and were found to be inhibitors with similar activity to CQ. The complexes also exhibit moderate to low cytotoxicity when evaluated against the Chinese Hamster Ovarian (CHO) cell-line *in vitro*, suggesting selectivity towards the malaria parasite rather than mammalian cells.

1. Introduction

Malaria is an infectious disease that affects millions of people every year. In 2016, 216 million cases of malaria were reported worldwide. Approximately 455,000 deaths occurred due to this disease in the same year [1]. In the past, chloroquine (CQ) has been the most widely used and most effective antimalarial. Since the emergence of chloroquine-resistant strains of malaria, this drug has been less effective. The increased resistance is associated with mutations in specific genes and proteins of malaria parasites, of which *Plasmodium falciparum* (*P. falciparum*) is the most well-studied species because of the high incidence of deaths caused by this parasite. An example of the occurrence of resistance is evident in the case of the *Plasmodium falciparum* CQ-resistance transporter (*Pf*CRT) protein. Mutations in the *Pf*CRT protein are believed to reduce the accumulation of chloroquine in the digestive vacuole of *Plasmodium falciparum* in CQ-resistant strains [2,3]. Since the emergence of resistant parasitic strains, drug discovery has been geared towards the development of alternative therapies that are able to overcome the resistance mechanisms experienced by CQ and many other quinoline-derived antimalarials. Artemisinin combination therapy (ACT) has been utilized in recent years to delay the development of resistance. In this regimen, one compound (usually a fast-acting artemisinin derivative) is used in combination with a second drug from a different compound class [4]. To date there have been reports of the emergence of ACT resistance, specifically in South-East Asia [5]. This further highlights the need for therapies with good efficacy against resistant parasite strains. Ferroquine, a metal-based derivative of chloroquine, displays potent activity in CQ-resistant strains that surpasses the activity of chloroquine. Ferroquine accumulates to a larger degree than CQ in the digestive vacuole of the *Plasmodium falciparum* parasite, mainly attributed to differences in its lipophilicity [6–8]. Since the discovery of ferroquine, the field of bioorganometallic chemistry has flourished, with much of the research aimed at the production of metallo-antimalarials [9–11]. Most of the complexes that have thus far been prepared and evaluated as antiplasmodial agents have been ferrocene-containing, with substantially less examples of platinum group metal complexes found in literature (Fig. 1) [10,12,13].

So-called RAPTA complexes have been investigated extensively as anticancer agents in recent years. These are compounds that usually contain a monodentate 1,3,5-triaza-phosphaadamantane (PTA) ligand as well as an η^6-arene ligand bound to a metal centre, usually ruthenium [14]. RAPTA complexes generally exhibit low in vitro

* Corresponding authors.
E-mail addresses: gregory.smith@uct.ac.za (G.S. Smith), ebbe.nordlander@chemphys.lu.se (E. Nordlander).

https://doi.org/10.1016/j.jinorgbio.2018.11.018
Received 22 September 2018; Received in revised form 15 November 2018; Accepted 25 November 2018
Available online 27 November 2018
0162-0134/

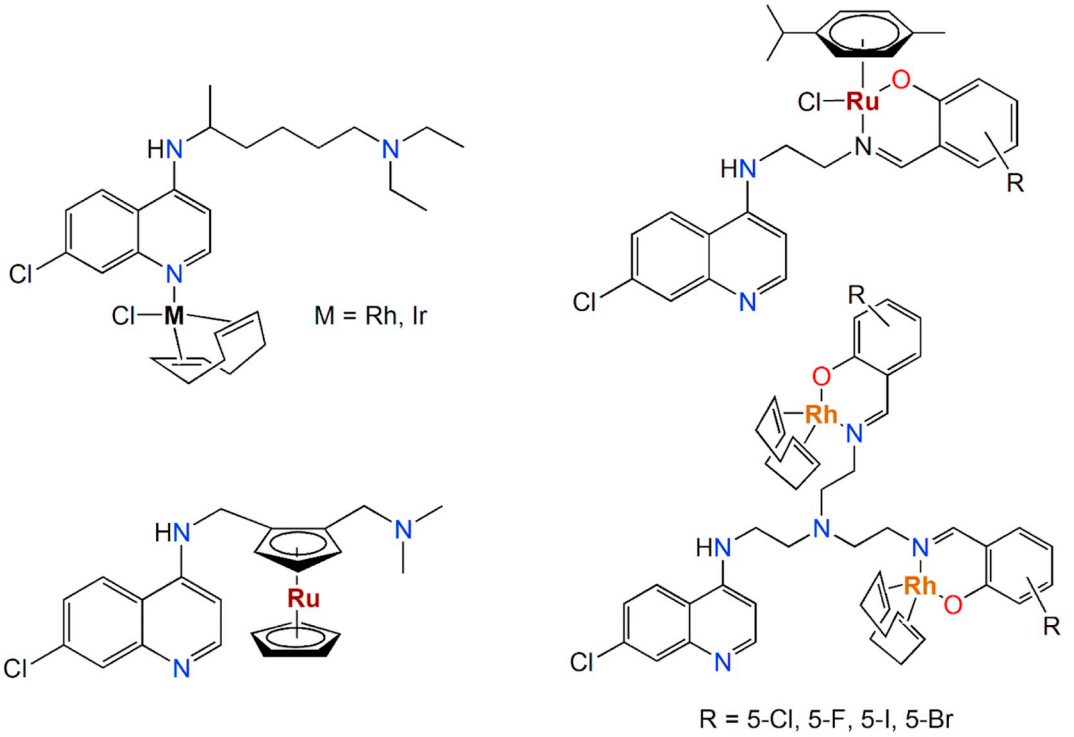

Fig. 1. A few examples of platinum group metal (PGM) complexes that have been investigated as antiplasmodial agents [10,12,13].

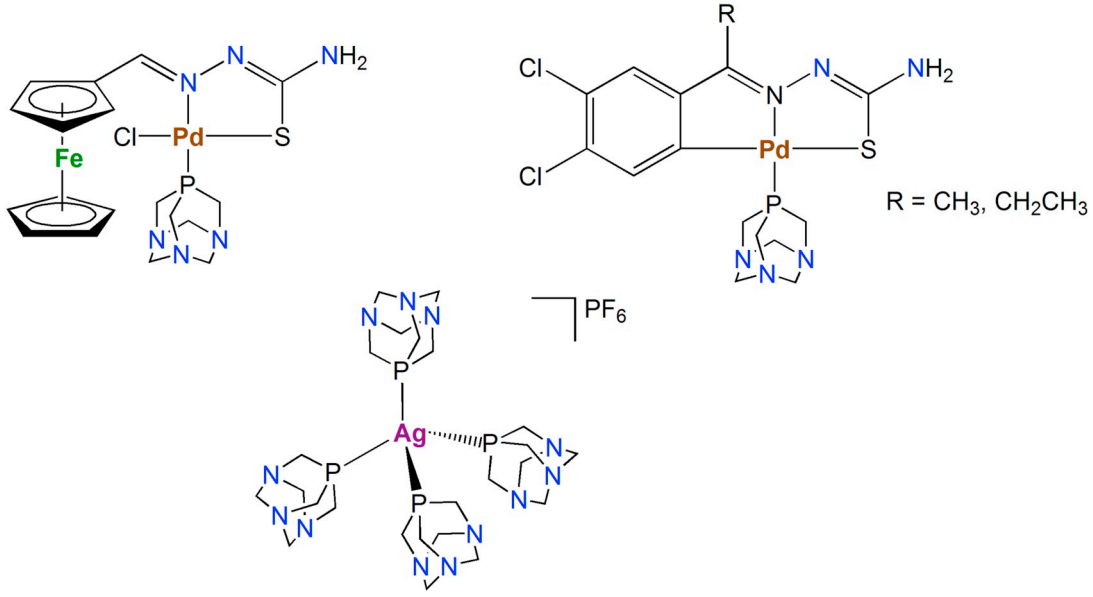

Fig. 2. Examples of PTA metal complexes evaluated for antimalarial activity [18–20].

cytotoxicities, but do inhibit lung metastasis in CBA mice [15,16]. Since this discovery, many analogues of RAPTA-type complexes have been prepared and evaluated as antitumor agents [17]. Only a few examples of PTA-containing metal complexes have been investigated as potential antimalarial agents (Fig. 2) [18–20]. This water-soluble phosphine is a desirable ligand to incorporate as part of antiplasmodial agents as it can be protonated at low pH, which is useful in terms of the malaria parasite, providing extra protonation sites in the digestive vacuole (DV) compared to CQ. The digestive vacuole of the malaria parasite is acidic, and protonation of PTA may result in enhanced pH trapping in the DV. In addition to this, the water-solubility of the PTA ligand would result in enhanced solubility in the testing medium. In this study we report on the synthesis, characterization, antiplasmodial and β-haematin inhibition activity of PTA-containing platinum group metal (PGM) complexes tethered to a 7-chloroquinoline moiety.

2. Results and discussion

2.1. Synthesis of the cationic complexes 1–12

A series of cationic ruthenium (**1–3**) and iridium (**4–6**) complexes were prepared from the previously reported neutral salicylaldiminato complexes **A–F** (Scheme 1) [13,21]. **A–F** were reacted in EtOH with PTA to afford the complexes (**1–6**) as yellow/orange solids in moderate yields (Scheme 1). The ruthenium complexes (**1–3**) were isolated as hexaflourophosphate salts after addition of NH_4PF_6. The iridium

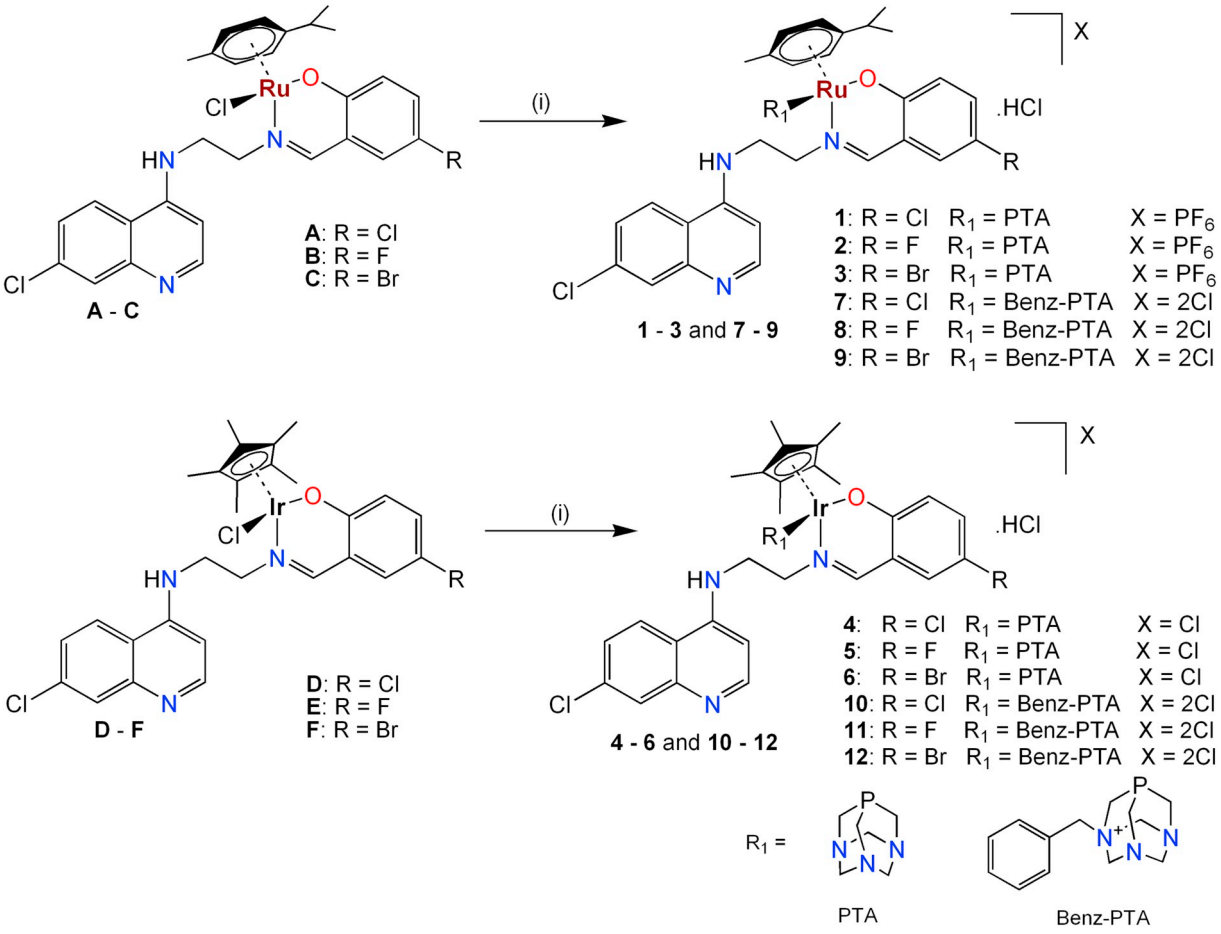

Scheme 1. Synthesis of ruthenium(II) and iridium(III) complexes (i) PTA (**1–6**) or benz-PTA (**7–12**) in EtOH or CH_2Cl_2, room temperature 1–8 h, NH_4PF_6 (**1–3**), room temperature, additional 1 h.

complexes (**4–6**) were isolated as chloride salts and are soluble in DMSO, MeOH and acetone. All compounds were characterized by nuclear magnetic resonance (NMR) spectroscopy, infrared (IR) spectroscopy and high-resolution electrospray ionization (HR-ESI) mass spectrometry. In the ^{1}H NMR spectra of the complexes (**1–6**), signals for the protons of the PTA ligand are observed in the region of 4–5 ppm, confirming its inclusion and overlapping with the signals of the protons of the ethylene chain anchored to the quinoline moiety. For the ruthenium complexes, signals for the *p*-cymene ligand are observed in the expected regions with four distinct signals observed for the *p*-cymene ring in the region of 5.6–6.5 ppm. Two signals are observed for the protons of the methyl groups of the isopropyl moiety in the region of 1.1–1.3 ppm, a consequence of the chiral nature of the ruthenium centre. For the iridium complexes (**4–6**), the signal for the Cp* ligand is observed as a doublet (Fig. S13), giving coupling constants of 1.95 Hz. This may be attributed to coupling of the protons of the Cp* ligand to the spin active phosphorus, which has been observed for similar complexes in the literature [22,23]. The infrared spectra of the complexes display bands in the region of 1576–1620 cm^{-1}, which are indicative of the C═N stretching frequencies. A series of cationic ruthenium (**7–9**) and iridium (**10–12**) complexes containing a benzyl-PTA ligand were also prepared from complexes **A–F**. This was done to investigate the effect on activity of including the benzyl-PTA ligand compared to the more water-soluble PTA ligand. The starting complexes **A–F** were reacted in dichloromethane with benzyl-PTA to afford complexes **7–12** in moderate yields (Scheme 1). The benzyl-PTA ligand was prepared from PTA and benzyl chloride according to published methods [24]. All the complexes were isolated as chloride salts. The ^{1}H NMR spectra confirmed that the desired complexes (**7–12**) were synthesized. Signals for the protons of the benzyl-PTA ligand and the methylene signals of the quinoline-salicylaldiminato ligands are observed in the region of 4–5 ppm, like their PTA counterparts. The main differences in the spectra are additional signals in the aromatic region accounting for the benzyl protons of the benzyl-PTA ligand. For ruthenium complexes **7–9**, a singlet for the phosphorus atom of the benzyl-PTA ligand occurs at approximately −12 ppm in the ^{31}P{^{1}H} NMR spectra, while for iridium complexes **10–12** the corresponding phosphorus signal occurs at −42 ppm.

2.2. Molecular structure of complex *10*

The molecular structure of complex **10** (Fig. 3) was also elucidated by single crystal X-ray diffraction. The relevant crystallographic data and refinement parameters are collated in Table 1. Selected bond angles and lengths are given in Table 2. Crystals were grown by diffusion of diethyl ether into a concentrated solution of complex **10** in methanol at room temperature. The compound crystallized in the triclinic $P\bar{1}$ space group with three methanol solvent molecules in the asymmetric unit. All non-hydrogen atoms were refined anisotropically.

The molecular structure shows coordination through the imine nitrogen and the phenolic oxygen donor atoms of the quinoline ligand in a bidentate manner to the iridium centre, forming a six-membered chelate ring. The additional sites are occupied by the alkylated PTA and Cp* ligands. The complex crystallizes as the hydrochloride salt of the quinoline moiety as is evident by the proton located on N3 and an adjacent chloride counterion (Cl1A, cf. Fig. 3). The complex also adopts the usual piano-stool geometry, with all bond lengths and angles around the metal centre being in the same range as other reported Cp*

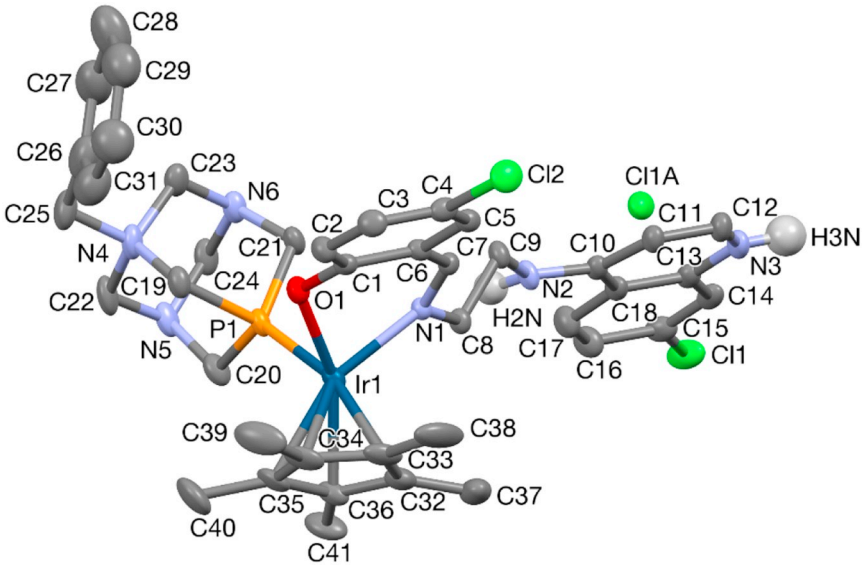

Fig. 3. A Mercury plot of the molecular structure of complex **10** and one chloride counterion. Thermal ellipsoids are plotted at the 30% level.

Table 1
Selected crystal data and structure refinement for complex **10**.

Complex	**10**
Empirical formula	$C_{41}H_{49}Cl_2IrN_6OP{\cdot}3CH_3O{\cdot}3Cl$
Formula weight	1135.40
Crystal system	Triclinic
Space group	$P\bar{1}$
Unit cell dimensions	
a (Å)	12.3137(17)
b (Å)	13.8158(18)
c (Å)	14.970(2)
α (°)	76.662(2)
β (°)	77.722(3)
γ (°)	81.964(2)
Volume (Å^3)	2410.3(6)
Z	2
Density (calculated, g·cm^{-3})	1.564
Absorption coefficient (mm^{-1})	3.127
F(000)	1146
Crystal size (mm)	0.07 × 0.12 × 0.17
Theta range for data collection (°)	1.9 to 28.0
Temperature (K)	173
Dataset	−16:16; −18:18; −19:19
Total reflections	42,684
Unique reflections [R(int.)]	11,483 [0.056]
Final R indices	R = 0.0450; wR_2 = 0.1088
Min. and max. residual density [e/Å^3]	−0.97 to 1.27

Table 2
Selected bond lengths (Å) and bond angles (°) for complex **10**.

Complex **10**	
Ir1−P1	2.2870(14)
Ir1−O1	2.090(4)
Ir1−N1	2.096(4)
Ir1−C32	2.207(6)
Ir1−C33	2.183(7)
Ir1−C34	2.205(6)
Ir1−C35	2.186(6)
Ir1−C36	2.190(6)
N2−H2N	0.97(4)
N3−H3N	0.97(5)
N1−C7	1.281(6)
P1−Ir1−O1	82.05(11)
P1−Ir1−N1	91.15(11)
O1−Ir1−N1	84.36(15)
Ir1−P1−C19	111.08(18)
C7−N1−C8	118.8(4)

complexes containing salicylaldimine ligands [21,25]. Bond distances for Ir1−P1, Ir1−O1 and Ir1−N1 are 2.2870(14), 2.090(4) and 2.096(4) Å, respectively. The imine (N1−C7) bond distance was found to be 1.281(6) and confirmation of the protonation of the quinoline nitrogen is confirmed by the N3-H3N bond distance (0.97(5) Å), which is consistent with the N2−H2N bond length.

2.3. Biological activity and mechanism

2.3.1. Antiplasmodial activity

Complexes **1–12** were screened for their antiplasmodial activity against two strains of *P. falciparum*, namely the NF54 CQ-sensitive (CQS) and K1 CQ-resistant (CQR) strains. The data obtained for these complexes are given in Table 3. The activity of the complexes was compared to the activity of previously synthesized complexes (**A–F**) [13,21] (Table 3. The data obtained for **A–F** from previous studies on the CQR Dd2 strain [13,21] are also given in the table.

In the CQS NF54 strain of *P. falciparum*, complexes **1-12** display potent activity, giving IC_{50} values well below 1 μM; however, these compounds are not as potent as the reference drug, CQ. Complex **2** and complex **10** have the most promising activity, with IC_{50} values in the low micromolar range similar to the rest of the complexes. In the chloroquine-resistant strain (K1), the complexes appear to lose their activity compared to the NF54 strain. The ruthenium complexes, specifically **1–3** and **8**, have higher IC_{50} values compared to their iridium counterparts. In the NF54 strain, the IC_{50} values obtained for the ruthenium complexes (**1–3**) are in the same range as similar neutral complexes investigated in a previous study [13]. This suggests that the addition of the PTA moiety does not greatly enhance the activity of these complexes in the sensitive strain compared to the neutral complexes. The IC_{50} values obtained for the iridium complexes (**4–6**), are about 10-fold higher compared to the corresponding neutral complexes prepared in a previous study for the same strain (NF54) [21]. For the ruthenium (**1–3**) and iridium (**4–6**) complexes, the trend with regard to the substituents show that the fluorine-containing (**2** and **5**) compounds are the most active in each case, followed by the chloro-derivatives (**1** and **4**) and then the bromo-substituted compounds (**3** and **6**). These trends are consistent with those observed for **A–F** evaluated previously [13,21]. Comparatively, the PTA complexes containing iridium as the metal are 10-fold less active than the neutral complexes **D–F**. This may

Table 3
Antiplasmodial activity of complexes **1–12** and **A–F** and CQ against the NF54, K1 and Dd2 strains of *P. falciparum*.

Compound	Metal	NF54 IC_{50} ± SE[a] (μM)	K1 IC_{50} ± SE (μM)	Dd2 IC_{50} ± SE (μM)	Resistance index (RI)[b]
1	Ru	0.33 ± 0.018	2.8 ± 0.093	–[c]	8
2	Ru	0.10 ± 0.069	3.8 ± 0.68	–	38
3	Ru	0.40 ± 0.035	4.5 ± 0.50	–	11
4	Ir	0.44 ± 0.055	1.6 ± 0.46	–	4
5	Ir	0.31 ± 0.038	1.7 ± 0.24	–	5
6	Ir	0.46 ± 0.068	1.1 ± 0.082	–	2
7	Ru	0.35 ± 0.019	1.5 ± 0.20	–	4
8	Ru	0.37 ± 0.063	4.2 ± 0.18	–	11
9	Ru	0.32 ± 0.022	1.6 ± 0.18	–	5
10	Ir	0.11 ± 0.015	1.2 ± 0.19	–	11
11	Ir	0.26 ± 0.027	1.0 ± 0.035	–	4
12	Ir	0.33 ± 0.10	1.1 ± 0.045	–	3
A	Ru	0.27	–[c]	1.08	4
B	Ru	0.14	–	0.66	4
C	Ru	0.49	–	1.44	3
D	Ir	0.058	–	0.27	5
E	Ir	0.030	–	0.26	9
F	Ir	0.084	–	0.30	4
CQ	–	0.031 ± 0.004	0.36 ± 0.07	0.22	12

[a] Standard error.
[b] Resistance index: IC_{50} (resistant strain)/IC_{50} (sensitive strain).
[c] Not determined.

be a consequence of the cationic nature of the synthesized complexes. Even though the compounds may possess enhanced aqueous solubility, this may affect the ability of the compounds to be transported into the DV of the parasite (possibly due to lower lipophilicity). The neutral complexes (**A–F**) and the PTA complexes prepared in the present study display cross-resistance when the activities are compared between the resistant (K1 or Dd2) and sensitive (NF54) strains. This observation indicates that incorporation of the metal does not provide a significant effect in overcoming the resistance mechanism of the quinoline moiety.

The benzyl-PTA ruthenium complexes (**7–9**) and benzyl-PTA iridium complexes (**10–12**) exhibit similar activity, with no substantial improvement or loss in activity when the alkylated PTA group is introduced. All the complexes display loss in activity in the K1 strain compared to the sensitive strain. The resistance index (RI) values were also determined to establish the degree of cross-resistance for these compounds compared to CQ. All the compounds appear to be cross-resistant giving RI values > 1. This suggests that the complexes may experience a similar resistance mechanism to that of CQ. Most of the iridium complexes (**4–6**, **11** and **12**), however, display lower RI values compared to CQ (Fig. 4) (albeit the complexes being less active), promoting the use of iridium Cp* complexes above the ruthenium *p*-cymene complexes in future drug design targeting resistance. Besides

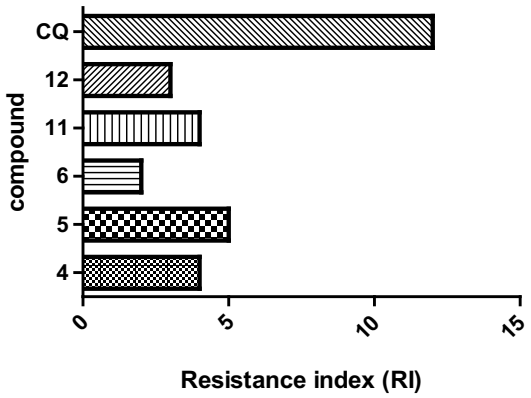

Fig. 4. Resistance index values of iridium complexes **4–6**, **11**, **12** and CQ.

Table 4
Cytotoxicity of **2**, **4**, **5**, **8**, **10** and emetine against CHO cells as well as the selectivity indices for the NF54 and K1 strains.

Compound	CHO IC_{50} (μM)	Selectivity Index (SI)[a]	Selectivity Index (SI)[b]
2	> 100	n.d.[c]	n.d.
4	15 ± 5	35	10
5	42 ± 5	136	25
8	> 100	n.d.	n.d.
10	16 ± 5	142	13
Emetine	0.036 ± 0.011	n.d.	n.d.

[a] Sensitive strain selectivity index: IC_{50} CHO/IC_{50} NF54.
[b] Resistant strain selectivity index: IC_{50} CHO/IC_{50} K1.
[c] Not determined.

the above-mentioned dependency of activity on halide substituent, no clear structure-activity trends could be observed for these complexes, which may be a consequence of various degrees of uptake into the digestive vacuole, due to the charged nature of the complexes.

2.3.2. Cytotoxicity

Selected complexes were screened for their *in vitro* cytotoxicity against Chinese Hamster Ovarian (CHO) cells to establish the toxicity of these complexes. Emetine was used as the control in these studies. The data obtained for this study is given in Table 4.

Overall, the complexes exhibited moderate to low toxicity when tested in this cell-line, compared to the reference drug, emetine. Specifically, the ruthenium complexes exhibit much lower toxicity compared to **4**, **5** and **10**, which are iridium compounds. With respect to the iridium complexes that were tested, the complex containing the fluoro-substituent (**5**) exhibits the lowest toxicity, with complexes **4** and **10** exhibiting similar activities. Overall, these complexes display good selectivity towards the malaria parasite, based on the selectivity index values being equal to 10 or more. This supports further optimization of these types of systems to target the malaria parasite.

2.3.3. β-Haematin inhibition studies

Chloroquine and other quinoline-containing compounds have been shown to inhibit haemozoin formation in the malaria parasite [26]. When a parasite invades a red blood cell of a human host, it digests haemoglobin as a food source. A toxic by-product of haemoglobin degradation is ferriprotoporphyrin(IX) or haematin, a pro-oxidant that generates oxidative stress, which is detrimental to the survival of the parasite. The parasite eliminates this threat by converting the toxic haematin into haemozoin (an insoluble, less toxic form) by a biocrystallization process [26,27]. Many quinoline antimalarials can inhibit the biocrystallization process of ferriprotoporphyrin, causing a build-up of the toxic haem species, resulting in death of the parasite. Since the complexes prepared in this study are quinoline-based, it is essential to establish whether these compounds act by the same mechanism of action as chloroquine (Fig. 5).

To determine experimentally whether the synthesized compounds may be haemozoin inhibitors in the parasite, it is possible to evaluate their ability to inhibit synthetic haemozoin (β-haematin) formation in a cell-free environment. β-Haematin formation can be evaluated using the NP-40 detergent-mediated assay [28]. NP-40 is a neutral detergent that mimics the lipids found in the biological system and facilitates the formation of β-haematin in the assay. Haemozoin formation is believed to occur in the presence of neutral lipids inside of the digestive vacuole of the parasite [29,30]. In the presence of higher concentrations of the quinoline compounds, the concentration of haemozoin should be lowered. In the assay, the amount of haematin is quantified using a colorimetric pyridine ferrochrome method developed by Ncokazi and Egan [31]. The ability of selected compounds to inhibit β-haematin formation was assessed using this detergent-mediated assay. The data obtained for this study are shown in Fig. 6. Complexes **1**, **5**, **7** and **8**, along

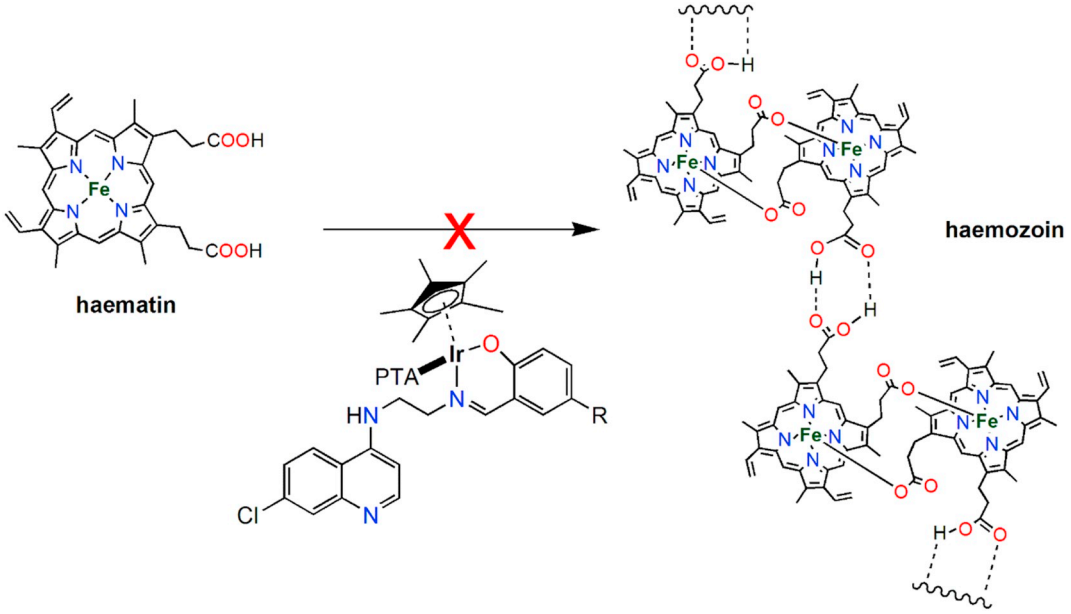

Fig. 5. Possible mechanism of action of complexes **1–12.**

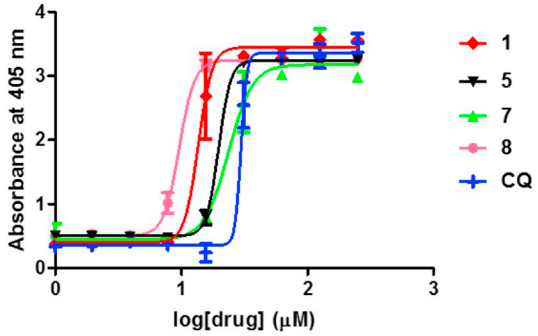

Fig. 6. Dose-response curves depicting the relationship between absorbance (proportional to haematin concentration) and compound concentration.

with CQ, were screened to determine whether these compounds share the same mechanism of action as CQ.

All tested compounds (**1**, **5**, **7**, **8** and CQ) inhibited synthetic haemozoin formation in the assay. The dose-response curves show a concentration-dependent increase in absorbance that corresponds to an increase in haematin concentration. At the highest drug concentration, the highest amount of haematin was observed, suggesting the inhibition of β-haematin formation. This suggests that these complexes are potentially haemozoin inhibitors in the parasite as well. However, no direct correlation between the antiplasmodial activity and the ability of the compounds to inhibit synthetic haemozoin formation can be established. This is a consequence of the β-haematin inhibition assay being a cell-free assay. Factors such as vacuolar accumulation, lipophilicity etc. (which all affect parasite inhibition activity) do not play a role in this experiment and hence no clear correlation is observed.

3. Conclusions

A series of cationic PTA-containing metal quinoline complexes (**1 − 12**) were prepared and characterized using standard spectroscopic and analytical techniques. The molecular structure of complex **10** was elucidated using single crystal X-ray diffraction analysis. The complex adopts the expected piano stool geometry and the structure confirms the cationic nature of the complexes. The compounds were screened for their antiplasmodial activity against the NF54 chloroquine (CQ)-sensitive and K1 CQ-resistant strains of *Plasmodium falciparum*. All the complexes display good activity in the CQ-sensitive strain, giving IC_{50} values < 1 μM, but suffer the same fate as CQ in the resistant strain (K1), resulting in decreased activity although some of the compounds exhibit lower resistance index (RI) values than the reference drug. In general, the iridium complexes exhibit lower RI values as well as slightly better activity in the K1 strain than the ruthenium complexes. Since the iridium complexes are less susceptible to cross-resistance (based on lower RI), the iridium Cp* moiety may be further exploited in future drug design. Complexes **2**, **4**, **5**, **8** and **10** were selected and screened against the CHO cell-line to establish selectivity. The complexes were found to be mildly cytotoxic, with the ruthenium complexes (**2** and **8**) displaying no notable toxicity at the tested concentration. Some fluoro-containing compounds (**2**, **5** and **8**) showed low toxicity. The selectivity indices obtained suggest that these complexes are selective towards the malaria parasite rather than mammalian cells. Selected compounds also showed the ability to inhibit β-haematin formation, suggesting that haemozoin may be the antiplasmodial target. This further encourages the use of this type of complexes in future drug design. In particular, iridium Cp* PTA complexes containing fluoro substituents appear to be prime candidates for further studies to optimize activity.

4. Experimental section

4.1. General

Synthetic procedures were performed in air at ambient temperatures unless otherwise stated. All reagents were purchased from Sigma Aldrich and used as received. Nuclear magnetic resonance (NMR) spectra were recorded on a Varian Inova 500 MHz spectrometer using the solvent resonance as internal standard. Infrared (IR) absorptions were measured on a Bruker Alpha-T FT-IR spectrometer using attenuated total reflectance (ATR). High resolution (HR) ESI-mass spectrometry was used to further characterize all new compounds and determinations were carried out using a Waters API Quattro instrument in the positive mode. The precursor complexes **A–F** [13,21] and the benzyl-PTA ligand [24] were synthesized following literature methods.

4.2. Synthesis of compounds

4.2.1. General synthesis procedures

The starting platinum group metal (PGM) quinoline complex was dissolved in EtOH or CH_2Cl_2 (50 ml). To this solution, 1,3,5-triaza-7-phosphaadamantane (PTA) or benzyl-PTA was added and the mixture stirred for 1–8 h at room temperature. After this time, the solvent was reduced under vacuum (to approx. 5 ml) to precipitate the chloride salt, which was filtered and washed with a minimal amount of cold EtOH or CH_2Cl_2, followed by diethyl ether. In the case of soluble products, after reduction of the solvent (to approx. 5 ml), NH_4PF_6 was added. The mixture was then stirred for an additional hour to yield a precipitate. The precipitate was then filtered, washed with EtOH, diethyl ether and dried *in vacuo*.

4.2.2. (η^6-p-Cymene)(N-(2-((5-chloro-2-hydroxyphenyl)methylimino) propyl)-7-chloroquinolin-4-amine)PTA ruthenium(II) hexafluorophosphate (1)

Ru-quinoline-Cl **A** (68.4 mg, 0.108 mmol), PTA (17.1 mg, 0.109 mmol) and NH_4PF_6 (18.0 mg, 0.110 mmol) were reacted in EtOH. Yield (35.3 mg, 36%). ^{1}H NMR (499.77 MHz, acetone-d_6): δ, ppm 1.11 (3H, d, J = 7 Hz, CH_3); 1.28 (3H, d, J = 7 Hz, CH_3); 2.29 (3H, s, CH); 2.62–2.69 (1H, m, CH); 4.25–4.67 (16H, m, CH_2); 5.62 (1H, d, J = 6 Hz, *p*-cy); 6.15–6.19 (1H, m, *p*-cy); 6.42 (1H, d, J = 6 Hz, *p*-cy); 6.54 (1H, t, J = 5 Hz, *p*-cy); 6.83 (1H, d, J = 10 Hz, ArH); 7.10 (1H, d, J = 6 Hz, ArH); 7.20–7.23 (2H, m, ArH); 7.60 (1H, dd, J = 2 Hz, 9 Hz, ArH); 8.02 (1H, d, J = 2 Hz, ArH); 8.36 (1H, d, J = 2 Hz, HC═N); 8.61 (1H, d, J = 6 Hz, ArH); 8.68–8.75 (1H, m, ArH); 9.29 (1H, br s, NH). ^{31}P{^{1}H} NMR (202.29 MHz, MeOD-d_4): −31.68 (s, PTA), −144.56 (sep, J = 709 Hz, PF_6). Microanalysis calculated for $C_{34}H_{41}Cl_3F_6N_6OP_2Ru{\cdot}3H_2O$: C 41.4; H 4.8; found C 41.5; H 3.9%. IR (ATR): ν, cm^{-1} 1613, 1591 (C═N). HR-ESI MS: *m/z* Found 751.1419 ([M-PF_6]$^+$); Calculated 751.1422.

4.2.3. (η^6-p-Cymene)(N-(2-((5-fluoro-2-hydroxyphenyl)methylimino) propyl)-7-chloroquinolin-4-amine)PTA ruthenium(II) hexafluorophosphate (2)

Ru-quinoline-F **B** (62.1 mg, 0.101 mmol), PTA (15.9 mg, 0.101 mmol) and NH_4PF_6 (17.3 mg, 0.106 mmol) were reacted in EtOH. Yield (64.2 mg, 72%). ^{1}H NMR (400.22 MHz, MeOD-d_4): δ, ppm 1.14 (3H, d, J = 7 Hz, CH_3); 1.29 (3H, d, J = 7 Hz, CH_3); 2.23 (3H, s, CH_3); 2.57–2.68 (1H, m, CH); 4.04–4.56 (16H, m, CH_2); 5.51 (1H, d, J = 6 Hz, *p*-cy); 5.83 (1H, d, J = 6 Hz, *p*-cy); 6.30 (1H, d, J = 6 Hz, *p*-cy); 6.32–6.37 (1H, m, *p*-cy); 6.82 (1H, dd, J = 4, 9 Hz, ArH); 6.87 (1H, dd, J = 3, 9 Hz, ArH); 7.04–7.13 (1H, m, ArH); 7.15 (1H, d, J = 7 Hz, ArH); 7.76 (1H, dd, J = 2, 9 Hz, ArH); 7.95 (1H, d, J = 2 Hz, ArH); 8.09 (1H, br s, HC═N); 8.50 (1H, d, J = 9 Hz, ArH); 8.53 (1H, d, J = 7 Hz, ArH). ^{31}P{^{1}H} NMR (202.29 MHz, acetone-d_6): −32.04 (s, PTA), −144.25 (sep, J = 708 Hz, PF_6). Microanalysis calculated for $C_{34}H_{41}Cl_2F_7N_6OP_2Ru{\cdot}2H_2O$: C 42.5; H 4.8; found C 42.1; H 4.4%. IR (ATR): ν, cm^{-1} 1615, 1592 (C═N). HR-ESI MS: *m/z* Found 735.1727 ([M-PF_6]$^+$); Calculated 735.1717.

4.2.4. (η^6-p-Cymene)(N-(2-((5-bromo-2-hydroxyphenyl)methylimino) propyl)-7-chloroquinolin-4-amine)PTA ruthenium(II) hexafluorophosphate (3)

Ru-quinoline-Br **C** (55.1 mg, 0.0817 mmol), PTA (12.8 mg, 0.0814 mmol) and NH_4PF_6 (14.0 mg, 0.858 mmol) were reacted in EtOH. Yield (38.3 mg, 50%). ^{1}H NMR (499.77 MHz, acetone-d_6): δ, ppm 1.13 (3H, d, J = 6.85, CH_3); 1.29 (3H, d, J = 6.85, CH_3); 2.28 (3H, s, CH_3); 2.61–2.69 (1H, m, CH); 4.20–4.65 (16H, m, CH_2); 5.62 (1H, d, J = 6 Hz, *p*-cy); 6.08–6.12 (1H, m, *p*-cy); 6.41 (1H, d, J = 5 Hz, *p*-cy); 6.55 (1H, t, J = 5 Hz, *p*-cy); 6.78 (1H, d, J = 9 Hz, ArH); 7.17 (1H, d, J = 7 Hz, ArH); 7.29–7.35 (2H, m, ArH); 7.70 (1H, d, J = 8 Hz, ArH); 8.05 (1H, s, ArH); 8.31 (1H, s, HC═N); 8.57 (1H, br s, ArH); 8.66 (1H, d, J = 6 Hz, ArH). ^{31}P{^{1}H} NMR (202.29 MHz, acetone-d_6): δ, ppm −31.78 (s, PTA), −144.56 (sep, J = 706 Hz, PF_6). Microanalysis calculated for $C_{34}H_{41}BrCl_2F_6N_6OP_2Ru{\cdot}3H_2O$: C 39.6; H 4.6; found C 39.2; H 4.0%. IR (ATR): ν, cm^{-1} 1612, 1597 (C═N). HR-ESI MS: *m/z* Found 797.0908 ([M-PF_6]$^+$); Calculated 797.0916.

4.2.5. (η^5-Pentamethylcyclopentadienyl) {(N-(2-((5-chloro-2-hydroxyphenyl)methylimino) propyl)-7-chloroquinolin-4-amine)}PTA iridium(III) chloride (4)

Ir-quinoline-Cl **D** (45.0 mg, 0.0623 mmol) and PTA (13.6 mg, 0.0636 mmol) were reacted in EtOH. Yield (21.0 mg, 38%). ^{1}H NMR (499.77 MHz, MeOD-d_4): δ, ppm 1.71 (15H, d, J = 2 Hz, Cp*); 3.89–4.11 (5H, m, CH_2); 4.17–4.32 (8H, m, CH_2); 4.43 (3H, d, J = 13 Hz, CH_2); 6.89–6.91 (2H, m, ArH); 7.33 (1H, dd, J = 3 Hz, 9 Hz, ArH); 7.40 (1H, d, J = 3 Hz, ArH); 7.50 (1H, dd, J = 2 Hz, 9 Hz, ArH); 7.86 (1H, d, J = 2 Hz, ArH); 8.15 (1H, d, J = 9 Hz, ArH); 8.31 (1H, br s, HC═N); 8.53 (1H, d, J = 5 Hz, ArH). ^{31}P{^{1}H} NMR (202.29 MHz, MeOD-d_4): δ, ppm −62.78 (s, PTA). Microanalysis calculated for $C_{34}H_{42}Cl_4IrN_6OP{\cdot}3H_2O$: C 42.1; H 4.9; found C 42.4; H 3.9%. IR (ATR): ν, cm^{-1} 1620, 1576 (C═N). HR-ESI MS: *m/z* Found 843.2070 ([M-Cl]$^+$); Calculated 843.2086.

4.2.6. (η^5-Pentamethylcyclopentadienyl) {(N-(2-((5-fluoro-2-hydroxyphenyl)methylimino) propyl)-7-chloroquinolin-4-amine)}PTA iridium(III) chloride (5)

Ir-quinoline-F **E** (61.8 mg, 0.0876 mmol) and PTA (14.3 mg, 0.0909 mmol) were reacted in EtOH. Yield (30.6 mg, 35%). ^{1}H NMR (499.77 MHz, MeOD-d_4): δ, ppm 1.71 (15H, d, J = 2 Hz, Cp*); 3.87–4.11 (5H, m, CH_2); 4.15–4.30 (8H, m, CH_2); 4.43 (3H, d, J = 14 Hz, CH_2); 6.87–6.91 (2H, m, ArH); 7.12 (1H, dd, J = 3 Hz, 9 Hz, ArH); 7.17–7.22 (1H, m, ArH); 7.48 (1H, dd, J = 2 Hz, 9 Hz, ArH); 7.86 (1H, d, J = 2 Hz, ArH); 8.10 (1H, d, J = 9 Hz, ArH); 8.28 (1H, br s, HC═N); 8.53 (1H, d, J = 5 Hz, ArH). ^{31}P{^{1}H} NMR (202.29 MHz, MeOD-d_4): δ, ppm −62.91 (s, PTA). Microanalysis calculated for $C_{34}H_{42}Cl_3FIrN_6OP$: C 45.4; H 4.7; found C 46.3; H 4.4%. IR (ATR): ν, cm^{-1} 1632, 1612 (C═N). HR-ESI MS: *m/z* Found 827.2371 ([M-Cl]$^+$); Calculated 827.2381.

4.2.7. (η^5-Pentamethylcyclopentadienyl) {(N-(2-((5-bromo-2-hydroxyphenyl)methylimino) propyl)-7-chloroquinolin-4-amine)}PTA iridium(III) chloride (6)

Ir-quinoline-Br **F** (55.1 mg, 0.0719 mmol) and PTA (11.9 mg, 0.0757 mmol) were reacted in EtOH. Yield (28.7 mg, 43%). ^{1}H NMR (499.77 MHz, MeOD-d_4): δ, ppm 1.72 (15H, d, J = 2 Hz, Cp*); 3.97–4.32 (14H, m, CH_2); 4.48 (2H, d, J = 13 Hz, CH_2); 6.86 (1H, d, J = 9 Hz, CH_2); 6.99 (1H, d, J = 6 Hz, ArH); 7.45 (1H, dd, J = 3 Hz, 9 Hz, ArH); 7.54 (1H, d, J = 2 Hz, ArH); 7.59 (1H, dd, J = 2 Hz, 9 Hz, ArH); 7.89 (1H, d, J = 2 Hz, ArH); 8.26 (1H, br s, ArH); 8.28 (1H, s, HC═N); 8.55 (1H, d, J = 6 Hz, ArH). ^{31}P{^{1}H} NMR (202.29 MHz, MeOD-d_4): δ, ppm −62.67 (s, PTA). Microanalysis for $C_{34}H_{42}BrCl_3IrN_6OP$: C 42.5; H 4.4; found: C 42.6; H 5.4%. IR (ATR): ν, cm^{-1} 1618, 1585 (C═N). HR-ESI MS: *m/z* Found 887.1556 ([M-Cl]$^+$); Calculated 887.1581.

4.2.8. (η^6-p-Cymene)(N-(2-((5-chloro-2-hydroxyphenyl)methylimino) propyl)-7-chloroquinolin-4-amine)benzPTA ruthenium(II) chloride (7)

Ru-quinoline-Cl **A** (26.3 mg, 0.0417 mmol) and benzyl-PTA (9.50 mg, 0.0334 mmol) were reacted in DCM for 4 h. Yield (14.6 mg, 48%). ^{1}H NMR (499.77 MHz, DMSO-d_6): δ, ppm 0.97 (3H, d, J = 7 Hz, CH_3); 1.15 (3H, d, J = 7 Hz, CH_3); 2.11 (3H, s, CH_3); 2.38–2.45 (1H, m, CH); 3.68–5.22 (18H, m, CH_2); 5.62 (1H, d, J = 6 Hz, *p*-cy); 6.26 (1H, d, J = 6 Hz, *p*-cy); 6.45 (1H, d, J = 6 Hz, *p*-cy); 6.57–6.63 (2H, m, *p*-cy, ArH); 7.04–7.55 (9H, m, ArH); 7.69 (1H, d, J = 8 Hz, ArH); 8.00 (1H, s, ArH); 8.26 (1H, s, HC═N); 8.63 (1H, d, J = 6 Hz, ArH); 8.87 (1H, br s, NH). ^{31}P{^{1}H} NMR (202.29 MHz, DMSO-d_6): δ, ppm −11.81 (s, benzPTA). Microanalysis calculated for $C_{41}H_{48}Cl_5N_6OPRu{\cdot}3.5CH_2Cl_2$: C 42.8; H 4.4; found C 42.2; H 4.7%. IR (ATR): ν, cm^{-1} 1609, 1578 (C═

N). HR-ESI MS: *m/z* Found 594.0648 ([M-Cl-benzPTACl]$^+$); Calculated 594.0653.

4.2.9. (η^6-p-Cymene)(N-(2-((5-fluoro-2-hydroxyphenyl)methylimino) propyl)-7-chloroquinolin-4-amine)benzPTA ruthenium(II) chloride (**8**)

Ru-quinoline-F **B** (50.2 mg, 0.0818 mmol) and benzyl-PTA (18.7 mg, 0.0659 mmol) were reacted in DCM for 4 h. Yield (25.2 mg, 43%). ^{1}H NMR (499.77 MHz, DMSO-d_6): δ, ppm 0.97 (3H, d, J = 7 Hz, CH_3); 1.13–1.17 (3H, m, CH_3); 2.10 (3H, s, CH_3); 2.40–2.45 (1H, m, CH); 3.73–5.21 (18H, m, CH_2); 5.62 (1H, d, J = 6 Hz, *p*-cy); 6.18 (1H, d, J = 5 Hz, *p*-cy); 6.42 (1H, d, J = 6 Hz, *p*-cy); 6.57–6.61 (2H, m, *p*-cy, ArH); 6.98 (1H, br s, ArH); 7.05–7.18 (2H, m, ArH); 7.22–7.29 (2H, m, ArH); 7.33–7.39 (2H, m, ArH); 7.42–7.60 (3H, m, ArH); 7.90 (1H, s, ArH); 8.22 (1H, s, HC═N); 8.55 (1H, d, J = 6 Hz, ArH); 8.64 (1H, br s, NH). ^{31}P{^{1}H} NMR (202.29 MHz, DMSO-d_6): δ, ppm −12.02 (s, benzPTA). Microanalysis calculated for $C_{41}H_{48}Cl_4FN_6OPRu{\cdot}2H_2O{\cdot}2CH_2Cl_2$: C 46.1; H 4.8; found C 46.5; H 5.8%. IR (ATR): ν, cm^{-1} 1611, 1579 (C═N). HR-ESI MS: *m/z* Found 578.0958 ([M-Cl-benzPTACl]$^+$); Calculated 578.0948.

4.2.10. (η^6-p-Cymene)(N-(2-((5-bromo-2-hydroxyphenyl)methylimino) propyl)-7-chloroquinolin-4-amine)benzPTA ruthenium(II) chloride (**9**)

Ru-quinoline-Br **C** (35.5 mg, 0.0526 mmol) and benzyl-PTA (14.5 mg, 0.0511 mmol) were reacted in DCM for 4 h. Yield (21.2 mg, 43%). ^{1}H NMR (499.77 MHz, DMSO-d_6): δ, ppm 0.98 (3H, d, J = 7 Hz, CH_3); 1.15 (3H, d, J = 7 Hz, CH_3); 2.12 (3H, s, CH_3); 2.38–2.45 (1H, m, CH); 3.74–5.23 (18H, m, CH_3); 5.63 (1H, d, J = 6 Hz, *p*-cy); 6.32 (1H, d, J = 6 Hz, *p*-cy); 6.46 (1H, d, J = 6 Hz, *p*-cy); 6.56 (1H, d, J = 9 Hz, ArH); 6.59–6.62 (1H, m, ArH); 7.21 (1H, d, J = 6 Hz, ArH); 7.27 (2H, d, J = 8 Hz, ArH); 7.32–7.39 (3H, m, ArH); 7.42–7.47 (1H, m, ArH); 7.50–7.54 (2H, m, ArH); 7.74 (1H, d, J = 8 Hz, ArH); 8.07 (1H, s, ArH); 8.28 (1H, s, ArH); 8.67 (1H, d, J = 7 Hz, ArH); 9.01 (1H, br s, NH). ^{31}P{^{1}H} NMR (202.29 MHz, DMSO-d_6): δ, ppm −11.79 (s, benzPTA). Microanalysis calculated for $C_{41}H_{48}BrCl_4N_6OPRu{\cdot}H_2O{\cdot}CH_2Cl_2$: C 45.9; H 4.7; found C 46.1; H 4.3%. IR (ATR): ν, cm^{-1} 1609, 1590 (C═N). HR-ESI MS: *m/z* Found 640.0122 ([M-Cl-benzPTACl]$^+$); Calculated 640.0148.

4.2.11. (η^5-Pentamethylcyclopentadienyl) {(N-(2-((5-chloro-2-hydroxyphenyl)methylimino) propyl)-7-chloroquinolin-4-amine)}benzPTA iridium(III) chloride (**10**)

Ir-quinoline-Cl **D** (46.2 mg, 0.0639 mmol) and benzyl-PTA (14.7 mg, 0.0518 mmol) were reacted in DCM for 8 h. Yield (30.8 mg, 59%). ^{1}H NMR (499.77 MHz, DMSO-d_6): δ, ppm 1.63 (15H, d, J = 2 Hz, Cp*); 4.00–4.28 (6H, m, CH_2); 4.38–4.52 (6H, m, CH_2); 4.60 (1H, d, J = 15 Hz, CH_2); 4.76 (1H, d, J = 14 Hz, CH_2); 5.07 (1H, d, J = 11 Hz, CH_2); 5.21 (2H, t, J = 13 Hz, CH_2); 5.31 (1H, d, J = 11 Hz, CH_2); 6.68 (1H, d, J = 9 Hz, ArH); 7.13 (1H, d, J = 5 Hz, ArH); 7.32–7.47 (7H, m, ArH); 7.62 (1H, d, J = 2 Hz, ArH); 7.69 (1H, d, J = 9 Hz, ArH); 8.02 (1H, s, ArH); 8.36 (1H, s, HC═N); 8.65 (1H, d, J = 6 Hz, ArH); 8.99 (1H, br s, NH). ^{31}P{^{1}H} NMR (202.29 MHz, DMSO-d_6): −42.17 (s, benzPTA). Microanalysis calculated for $C_{41}H_{49}Cl_5IrN_6OP{\cdot}4.5H_2O$: C 43.8; H 5.2; found C 43.7; H 5.0%. IR (ATR): ν, cm^{-1} 1628, 1611 (C═N). HR-ESI MS: *m/z* Found 969.2297 ([M-Cl]$^+$); Calculated 969.2322.

4.2.12. (η^5-Pentamethylcyclopentadienyl){(N-(2-((5-fluoro-2-hydroxyphenyl)methylimino)propyl)-7-chloroquinolin-4-amine)}benzPTA iridium(III) chloride (**11**)

Ir-quinoline-F **E** (43.6 mg, 0.0618 mmol) and benzyl-PTA (14.3 mg, 0.0504 mmol) were reacted in DCM for 8 h. Yield (38.2 mg, 77%). ^{1}H NMR (499.77 MHz, DMSO-d_6): δ, ppm 1.62 (15H, d, J = 2 Hz, Cp*); 3.90–4.72 (14H, m, CH_2); 5.07 (1H, d, J = 12 Hz, CH_2); 5.15–5.26 (3H, m, CH_2); 6.64–6.69 (1H, m, ArH); 6.99 (1H, br s, ArH); 7.22–7.29 (1H, m, ArH); 7.35–7.48 (7H, m, ArH); 7.60 (1H, d, J = 9 Hz, ArH); 7.93 (1H, s, ArH); 8.33 (1H, s, HC═N); 8.60 (1H, d, J = 6 Hz, ArH); 8.77 (1H, br s, NH). ^{31}P{^{1}H} NMR (202.29 MHz, acetone-d_6): −42.54 (s, benzPTA). Microanalysis calculated for $C_{41}H_{49}Cl_4FIrN_6OP{\cdot}3H_2O$: C 45.6; H 5.1; found C 45.4; H 5.6%. IR (ATR): ν, cm^{-1} 1612, 1579 (C═N). HR-ESI MS: *m/z* Found 953.2592 ([M-Cl]$^+$); Calculated 953.2618.

4.2.13. (η^5-Pentamethylcyclopentadienyl) {(N-(2-((5-bromo-2-hydroxyphenyl)methylimino) propyl)-7-chloroquinolin-4-amine)}benzPTA iridium(III) chloride (**12**)

Ir-quinoline-Br **F** (40.0 mg, 0.0522 mmol) and benzyl-PTA (11.8 mg, 0.0417 mmol) were reacted in DCM for 8 h. Yield (28.1 mg, 64%). ^{1}H NMR (499.77 MHz, DMSO-d_6): δ, ppm 1.62 (15H, d, J = 2 Hz, Cp*); 3.98–4.24 (6H, m, CH_2); 4.36–4.51 (6H, m, CH_2); 4.53–4.61 (1H, m, CH_2); 4.74 (1H, d, J = 14 Hz, CH_2); 5.04 (1H, d, J = 11 Hz, CH_2); 5.19 (2H, t, J = 11 Hz, CH_2); 5.29 (1H, d, J = 10 Hz, CH_2); 6.62 (1H, d, J = 9 Hz, ArH); 7.11 (1H, br s, ArH); 7.33–7.46 (7H, m, ArH); 7.69 (1H, d, J = 9 Hz, ArH); 7.72 (1H, d, J = 2 Hz, ArH); 7.99 (1H, s, ArH); 8.33 (1H, s, HC═N); 8.65 (1H, d, J = 7 Hz, ArH); 8.96 (1H, br s, NH). ^{31}P{^{1}H} NMR (202.29 MHz, DMSO-d_6): −42.07 (s, benzPTA). IR (ATR): ν, cm^{-1} 1627, 1610 (C═N). HR-ESI MS: *m/z* Found 1015.1815 ([M-Cl]$^+$); Calculated 1015.1817.

4.3. In vitro antiplasmodial assay

The samples were tested in triplicate against the chloroquine-sensitive NF54 strain and chloroquine-resistant K1 strain of *P. falciparum*. Continuous *in vitro* cultures of asexual erythrocyte stages of *P. falciparum* were conserved using a modified method of Trager and Jensen [32]. The antiplasmodial activity was determined *in vitro* via the parasite lactate dehydrogenase assay using a modified method described by Makler *et al.* [33]. The samples were prepared as a 2 mg ml^{-1} stock solution using DMSO and sonicated to enhance solubility. Stock solutions were stored at −20 °C. Further dilutions were prepared on the day of the experiment. Chloroquine diphosphate was used as the standard in all experiments. A full dose-response measurement was performed for all compounds to determine the concentration inhibiting 50% of parasite growth (IC_{50} value). The samples were tested at a starting concentration of 10,000 ng ml^{-1}, which was then serially diluted 2-fold in complete medium to give 10 concentrations. The same dilution technique was used for all samples. The parasite was exposed to the test samples for 48 h. The highest concentration of solvent to which the parasites were exposed to had no measurable effect on the parasite viability. The IC_{50} values were obtained using a nonlinear dose-response curve fitting analysis via Graph Pad Prism v.5.0 software.

4.4. In vitro cytotoxicity

Test samples were screened for *in vitro* cytotoxicity against a mammalian cell-line, Chinese Hamster Ovarian (CHO), using the 3-(4,5-dimethylthiazol-2-yl)-2,5-diphenyltetrazolium bromide (MTT)-assay. The MTT-assay is used as a colorimetric assay for cellular growth and survival, and compares well with other available assays [34,35]. The tetrazolium salt MTT was used to measure all growth and chemosensitivity. The tetrazolium ring is cleaved in active mitochondria. Thus only viable cells are able to reduce the water-soluble yellow colored MTT to water-insoluble purple colored formazan. Formazan crystals are dissolved in dimethyl sulfoxide (DMSO). The test samples were tested in triplicate on one occasion. The test samples were prepared to a 20 mg ml^{-1} stock solution in 100% DMSO. Stock solutions were stored at −20 °C. Further dilutions were prepared in complete medium on the day of the experiment. Samples were tested as a suspension if not completely dissolved. Emetine was used as the reference drug in all experiments. The initial concentration of emetine was 100 μg ml^{-1}, which was diluted in complete medium with 10-fold dilutions to give 6 concentrations, the lowest being 0.001 μg ml^{-1}. The same dilution technique was applied to all test samples. The cells were incubated in the presence of the drug for 48 h. The highest concentration of solvent to which the cells were exposed to had no measurable effect on the cell

viability. The 50% inhibitory concentration (IC_{50}) values were obtained from full dose–response curves, using a non-linear dose–response curve fitting analysis via GraphPad Prism v.5 software.

4.5. β-Haematin inhibition assay

The β-haematin assay was adapted from the method described by Wright and co-workers [28]. Compounds were prepared as a 10 mM stock solution in 100% DMSO. Samples were tested at a starting concentration of 500 µM. The stock solution was serially diluted to give 12 concentrations in a 96 well flat-bottom assay plate. NP-40 detergent was added to mediate the formation of β-haematin (30.55 µM, final concentration). A 25 mM stock solution of haematin was prepared by dissolving hemin (16.3 mg) in DMSO (1 mL). A 177.76 µl aliquot of haematin stock was suspended in 20 ml of acetate buffer adjusted to pH 4.7. The haematin suspension was then added to the plate to give a final haematin concentration of 100 µM. The plate was incubated for 16 h at 37 °C. The compounds were analyzed using the pyridine ferrochrome method developed by Ncokazi and Egan [31]. 32 µl of a solution of 50% pyridine, 20% acetone, 20% water, and 10% 2 M HEPES buffer (pH 7.4) was added to each well. To this, 60 µl acetone was then added to each well and mixed. The absorbance of the resulting complex was measured at 405 nm on a SpectraMax 340PC plate reader. The IC_{50} values were obtained using a non-linear dose-response curve fitting analysis via Graph Pad Prism v.5.0 software.

4.6. Single-crystal X-ray diffraction studies

Single-crystal X-ray diffraction data were collected on a Bruker KAPPA APEX II DUO diffractometer using graphite-monochromated Mo-Kα radiation (χ = 0.71073 Å). Data collection was carried out at 173(2) K. The temperature was controlled by an Oxford Cryostream cooling system (Oxford Cryostat). Cell refinement and data reduction were performed using the program SAINT [36]. The data were scaled and absorption corrections performed using SADABS [37]. The structure was solved by direct methods using SHELXS-97 [37] and refined by full-matrix least-squares methods based on F2 using SHELXL-2014 [37] and using the graphics interface program X-Seed [38,39]. The programs X-Seed and POV-Ray [40] were used to prepare molecular graphic images. All non-hydrogen atoms were refined anisotropically. All hydrogens, except H2N on N2, H3N on N3 and three hydroxyl hydrogens of the methanol solvent molecules, were placed in idealized positions using the build-in functions of SHELXL and refined in riding models with U_{iso} assigned 1.2 or 1.5 times U_{eq} of their parent atoms and the bond distances were constrained to 0.95 Å for the aromatic hydrogens, 0.98 Å for the methyl hydrogens and 0.99 Å for –CH2. The positions of H2N and H3N were located in the Difference Electron Density Maps and were refined with simple bond length constraints [Distance (N−H) = 0.970(2) Å]. The hydroxyl hydrogens of the three methanol solvent molecules could not be located and were excluded from the structure model. The structure was refined to an R factor of 0.0450.

Abbreviations

ACT	artemisinin combination therapy
CHO	Chinese Hamster Ovarian
CQ	chloroquine
CQR	chloroquine-resistant
CQS	chloroquine-sensitive
DV	digestive vacuole
IR	infrared
HR-ESI	high resolution electrospray ionization
MTT	3-(4,5-dimethylthiazol-2-yl)-2,5-diphenyltetrazolium bromide
NMR	nuclear magnetic resonance
*Pf*CRT	*Plasmodium falciparum* CQ resistance transporter
PGM	platinum group metal
PTA	1,3,5-triaza-phosphaadamantane
RI	resistance index

Acknowledgements

TS thanks the Crafoord Foundation for a postdoctoral fellowship. GSS thanks the University of Cape Town and the National Research Foundation of South Africa (UID: 111707) for financial support.

Appendix A. Supplementary data

CCDC 1862269 contains the supplementary crystallographic data for this paper. This data can be obtained free of charge from The Cambridge Crystallographic Data Centre via www.ccdc.cam.ac.uk/data_request/cif. Supplementary data related to this article can be found at https://doi.org/10.1016/j.jinorgbio.2018.11.018.

References

[1] World Malaria Report, (2017) (Geneva, Switzerland).
[2] A. Ecker, A.M. Lehane, J. Clain, D.A. Fidock, Trends Parasitol. 28 (2012) 504–514.
[3] D.A. Fidock, T. Nomura, A.K. Talley, R.A. Cooper, S.M. Dzekunov, M.T. Ferdig, L.M.B. Ursos, A.B.S. Sidhu, B. Naude, K.W. Deitsch, X.Z. Su, J.C. Wootton, P.D. Roepe, T.E. Wellems, Mol. Cell 6 (2000) 861–871.
[4] Artemisinin-based Combination Therapy, https://www.malariaconsortium.org/pages/112.htm , Accessed date: 25 March 2018.
[5] Global Malaria Programme status report, Artemisinin and Artemisinin-based Combination Therapy Resistance, 2017.
[6] C. Biot, G. Glorian, L.A. Maciejewski, J.S. Brocard, O. Domarle, G. Blampain, P. Millet, A.J. Georges, H. Abessolo, D. Dive, J. Lebibi, J. Med. Chem. 40 (1997) 3715–3718.
[7] F. Dubar, C. Slomianny, J. Khalife, D. Dive, H. Kalamou, Y. Guerardel, P. Grellier, C. Biot, Angew. Chem. Int. Ed. 52 (2013) 7690–7693.
[8] F. Dubar, T.J. Egan, B. Pradines, D. Kuter, K.K. Ncokazi, D. Forge, J.F. Paul, C. Pierrot, H. Kalamou, J. Khalife, E. Buisine, C. Rogier, H. Vezin, I. Forfar, C. Slomianny, X. Trivelli, S. Kapishnikov, L. Leiserowitz, D. Dive, C. Biot, ACS Chem. Biol. 6 (2011) 275–287.
[9] C. Biot, D. Dive, Top. Organomet. Chem. 32 (2010) 155–193.
[10] P.F. Salas, C. Herrmann, C. Orvig, Chem. Rev. 113 (2013) 3450–3492.
[11] M. Navarro, W. Castro, C. Biot, Organometallics 31 (2012) 5715–5727.
[12] T. Stringer, D. Taylor, H. Guzgay, A. Shokar, A. Au, P.J. Smith, D.T. Hendricks, K.M. Land, T.J. Egan, G.S. Smith, Dalton Trans. 44 (2015) 14906–14917.
[13] E. Ekengard, L. Glans, I. Cassells, T. Fogeron, P. Govender, T. Stringer, P. Chellan, G.C. Lisensky, W.H. Hersh, I. Doverbratt, S. Lidin, C. de Kock, P.J. Smith, G.S. Smith, E. Nordlander, Dalton Trans. 44 (2015) 19314–19329.
[14] G. Süss-Fink, Dalton Trans. 39 (2010) 1673–1688.
[15] C. Scolaro, A. Bergamo, L. Brescacin, R. Delfino, M. Cocchietto, G. Laurenczy, T.J. Geldbach, G. Sava, P.J. Dyson, J. Med. Chem. 48 (2005) 4161–4171.
[16] A. Bergamo, A. Masi, P.J. Dyson, G. Sava, Int. J. Oncol. 33 (2008) 1281–1289.
[17] L. Zeng, P. Gupta, Y.L. Chen, E. Wang, L. Ji, H. Chao, Z.-S. Chen, Chem. Soc. Rev. 46 (2017) 5771–5804.
[18] M. Adams, C. de Kock, P.J. Smith, K. Chibale, G.S. Smith, J. Organomet. Chem. 736 (2013) 19–26.
[19] M. Adams, C. de Kock, P.J. Smith, P. Malatji, A.T. Hutton, K. Chibale, G.S. Smith, J. Organomet. Chem. 739 (2013) 15–20.
[20] S. Tapanelli, A. Habluetzel, M. Pellei, L. Marchiò, A. Tombesi, A. Capparè, C. Santini, J. Inorg. Biochem. 166 (2017) 1–4.
[21] E. Ekengard, K. Kumar, T. Fogeron, C. de Kock, P.J. Smith, M. Haukka, M. Monari, E. Nordlander, Dalton Trans. 45 (2016) 3905–3917.
[22] A.R. Burgoyne, C.H. Kaschula, M.I. Parker, G.S. Smith, Eur. J. Inorg. Chem. (2016) 1267–1273.
[23] M. Nomura, M. Fourmigué, Inorg. Chem. 47 (2008) 1301–1312.
[24] F.X. Legrand, F. Hapiot, S. Tilloy, A. Guerriero, M. Peruzzini, L. Gonsalvi, E. Monflier, Appl. Catal. 362 (2009) 62–66.
[25] R. Payne, P. Govender, B. Therrien, C.M. Clavel, P.J. Dyson, G.S. Smith, J. Organomet. Chem. 729 (2013) 20–27.
[26] T.J. Egan, Expert Opin. Ther. Pat. 11 (2001) 185–209.
[27] M. Foley, L. Tilley, Pharmacol. Therapeut. 79 (1998) 55–87.
[28] R.D. Sandlin, M.D. Carter, P.J. Lee, J.M. Auschwitz, S.E. Leed, J.D. Johnson, D.W. Wright, Antimicrob. Agents Chemother. 55 (2011) 3363–3369.
[29] A.N. Hoang, K.K. Ncokazi, K.A. de Villiers, D.W. Wright, T.J. Egan, Dalton Trans. 39 (2010) 1235–1244.
[30] A.N. Hoang, R.D. Sandlin, A. Omar, T.J. Egan, D.W. Wright, Biochemistry 49 (2010)

10107–10116.
[31] K.K. Ncokazi, T.J. Egan, Anal. Biochem. 338 (2005) 306–319.
[32] W. Trager, J.B. Jensen, Science 193 (1976) 673–675.
[33] M.T. Makler, J.M. Ries, J.A. Williams, J.E. Bancroft, R.C. Piper, B.L. Gibbins, D.J. Hinrichs, Am. J. Trop. Med. Hyg. 48 (1993) 739–741.
[34] T. Mosmann, J. Immunol. Methods 65 (1983) 55–63.
[35] L.V. Rubinstein, R.H. Shoemaker, K.D. Paull, R.M. Simon, S. Tosini, P. Skehan, D.A. Scudiero, A. Monks, M.R. Boyd, J. Natl. Cancer Inst. 82 (1990) 1113–1118.
[36] SAINT Version 7.60a, Bruker AXS Inc., Madison, WI, USA, 2006.
[37] G.M. Sheldrick, SHELXS-97, SHELXL-2014 and SADABS Version 2.05, University of Göttingen, Germany, 1997.
[38] L.J. Barbour, J. Supramol. Chem. 1 (2001) 189–191.
[39] J.L. Atwood, L.J. Barbour, Molecular graphics: from science to art, Cryst. Growth Des. 3 (2003) 3–8.
[40] http://www.povray.org (accessed 20 July 2018).